doi:10.2533/chimia.2017.7 Chimia 71 (2017) 7–12 © Swiss Chemical Society

Measuring Intermolecular Binding Energies by Laser Spectroscopy

Richard Knochenmuss[a], Surajit Maity[b], Géraldine Féraud[c], and Samuel Leutwyler*[a]

Abstract: The ground-state dissociation energy, $D_0(S_0)$, of isolated intermolecular complexes in the gas phase is a fundamental measure of the interaction strength between the molecules. We have developed a three-laser, triply resonant pump-dump-probe technique to measure dissociation energies of jet-cooled M•S complexes, where M is an aromatic chromophore and S is a closed-shell 'solvent' molecule. Stimulated emission pumping (SEP) *via* the $S_0 \leftrightarrow S_1$ electronic transition is used to precisely 'warm' the complex by populating high vibrational levels v" of the S_0 state. If the deposited energy E(v") is less than $D_0(S_0)$, the complex remains intact, and is then mass- and isomer-selectively detected by resonant two-photon ionization (R2PI) with a third (probe) laser. If the pumped level is above $D_0(S_0)$, the hot complex dissociates and the probe signal disappears. Combining the fluorescence or SEP spectrum of the cold complex with the SEP breakoff of the hot complex brackets $D_0(S_0)$. The UV chromophores 1-naphthol and carbazole were employed; these bind either dispersively *via* the aromatic rings, or form a hydrogen bond *via* the -OH or -NH group. Dissociation energies have been measured for dispersively bound complexes with noble gases (Ne, Kr, Ar, Xe), diatomics (N_2, CO), alkanes (methane to n-butane), cycloalkanes (cyclopropane to cycloheptane), and unsaturated compounds (ethene, benzene). Hydrogen-bond dissociation energies have been measured for H_2O, D_2O, methanol, ethanol, ethers (oxirane, oxetane), NH_3 and ND_3.

Keywords: Dispersive interactions · Hydrogen bonding · Intermolecular interactions · Stimulated emission pumping

1. Introduction

Spectroscopic methods for determining dissociation energies, D_0, of diatomic and triatomic molecules have a long and illustrious history. Early techniques such as the Birge-Sponer extrapolation[1] determine the D_0 of a diatomic molecule by assuming a specific vibrational potential function (*e.g.* Morse[2] or R^{-6}). A series of spectroscopically measured and assigned vibrational transitions can then be extrapolated to the dissociation limit for AB→ A˙ + B˙.[3,4] More recently, the dissociation energy of the HO–H bond in the water molecule has been measured by a triply-resonant scheme employing a series of vibrational overtone transitions. This gave direct spectroscopic access to the onset of the $H_2O \rightarrow H^{\cdot} + OH^{\cdot}$ dissociation continuum.[5,6]

For larger molecules, sequential up-pumping is impractical due to the complexity of assigning high vibrational-rotational levels of multidimensional potential energy surfaces. Furthermore, intramolecular vibrational relaxation (IVR) from higher vibrational levels becomes faster than the achievable up-pumping rates. To bypass such difficulties, we take advantage of properties of our target species, M•S intermolecular complexes, where M is a UV chromophore and S is a closed-shell 'solvent' molecule.

In this scheme,[7–12] high M•S *inter*-molecular vibrational levels are indirectly excited *via intra*molecular vibrational levels of the chromophore, M. These could, in principle, be directly accessed in the infrared region, but the relatively low IR absorption cross-sections and the restricted tuning range of IR lasers make it more effective to use a pump-dump strategy, also called stimulated-emission pumping (SEP). As seen in Fig. 1, a first UV laser transfers (pumps) ground-state population to the vibrationless (v'=0) first electronic excited state of M•S. Shortly thereafter, a second UV laser transfers population down (dump, violet-green downward arrows) to vibrational levels (v") of M•S in the electronic ground state (thick black lines). The pump and dump transitions are in the UV and have high oscillator strengths, so the process is relatively efficient. The v" level of M undergoes IVR to intermolecular modes of the complex (thin gray lines), on a timescale of nanoseconds to microseconds. If the energy deposited in the now 'hot' M*•S complex is larger than $D_0(S_0)$, it undergoes vibrational predissociation to M and S. Otherwise it remains intact and can be detected by resonant 2-photon ionization (R2PI, a third laser) and mass spectrometry.[7,13]

The dissociation energy is bracketed by comparing two measurements. The R2PI probe laser can be set to specifically detect hot M*•S by exciting on so-called 'hot bands'. When the dump laser is scanned, peaks appear at the v" energies of M*•S, but break off when v" is above D_0. This corresponds to the gold spectrum on the right of Fig. 1. The last peak in this spectrum is a lower limit for the dissociation energy.

To find the upper limit for D_0, two methods are used. First, the probe laser can be set to monitor cold M•S while the dump is scanned. Since the dump process heats the complex, it depletes the cold signal, regardless of whether the complexes dissociate or not. This is called a dump spectrum. Alternatively the fluorescence emission spectrum from the first singlet excited state (S_1) can be measured, since it also does not depend on whether the lower state dissociates. This is shown as the blue spectrum on the left of Fig. 1. The first peak above the previously identified lower limit is the upper limit for D_0.

*Correspondence: Prof. Dr. S. Leutwyler[a]
E-Mail: leutwyler@iac.unibe.ch
[a]Universität Bern
Departement für Chemie und Biochemie
Freiestrasse 3
CH-3012 Bern
[b]Current address: Dept. of Chemistry, IIT Hyderabad
Kandi, Sangareddy-502285, Telangana, India
[c]Current address: LERMA, Sorbonne Universités
UPMC University Paris 06, Observatorie de Paris
PSL Research University, CNRS, F-75252 Paris

Fig. 2 shows the pump-dump-IVR effect in the 1-naphthol•cycloheptane complex. The black spectrum is the normal 1-color R2PI spectrum in the $S_0 \rightarrow S_1$ origin region. If the pump laser is then fixed on the isomer B origin, many ground-state complexes are up-pumped and lost. The blue spectrum shows this depletion of both the isomer B origin and vibronic bands. When the dump is added, also at the isomer B origin, not only is the depletion more extensive, but also a broad absorption appears below the origins (red spectrum and shaded area). These are the hot-band transitions of the vibrationally excited complexes.

Fig. 3 is an example of a bracketing experiment on 1-naphthol•cyclohexane. The probe laser is first fixed on hot bands, as indicated in Fig. 2, while the dump is scanned. The signal of the R2PI ionized complex is observed with the mass spectrometer. This produces a spectrum like the upper, gold, trace in Fig. 3. The arrow indicates the last peak for which the complex remains intact. In this case, a dump spectrum of cold complexes was used for the comparative measurement, as shown by the blue trace. The dump spectrum is not inverted, the peaks are negative, indicating depletion. The two arrows show the bracket of D_0 for this cluster, between 1697 and 1703 cm^{-1}.

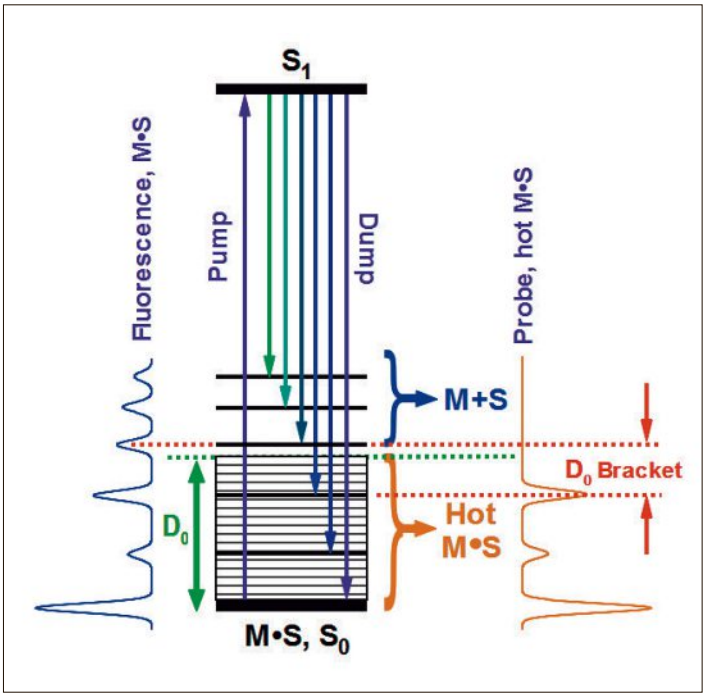

Fig. 1. Stimulated-emission pumping part of the SEP-R2PI experiment of an M•S complex: Following the pump step at the $S_1 \leftarrow S_0$ origin, the excited M•S complex either fluoresces back to many different S_0 state vibrational levels (fluorescence spectrum on the left) or is dumped to a specific v'' level in the S_0 state (violet to green vertical arrows). The hot M•S complex is detected by a third 'probe' laser (not shown), this is the gold SEP spectrum on the right. Note that the SEP spectrum breaks off as soon as the hot v'' level of M•S lies above D_0, leading to vibrational predissociation: M•S → M + S. The intermolecular dissociation energy $D_0(S_0)$ is bracketed by the highest v'' level observed in the SEP spectrum and the next vibrational level that is observed in the fluorescence spectrum on the left.

2. Noble Gas Complexes

Weakly bound van der Waals complexes between aromatics and noble-gas (NG) atoms are prototypical for the investigation of non-polar solvation and the buildup of solvent shells. The main attractive interaction of an aromatic with a noble-gas atom is quantum mechanical dispersion. In the limit of two interacting atoms, and expanded in terms of polarizability moments, the dominant dispersion term is from the dipole polarizabilities, which falls off as R^{-6}, where R is the interatomic distance. The next term is the dipole-quadrupole polarizability contribution, with an R^{-8} dependence. The complexes of carbazole with NG = Ne, Ar, Kr and Xe offer a systematic test of this and other theories of dispersion.

Ground-state dissociation energies of carbazole•NG were determined by the SEP-R2PI method[10] as shown in Fig. 4. Except for Ne, the relative uncertainty was <0.4%. For the Ne complex only an upper limit could be determined, the lower limit was estimated. The carbazole-NG distances have not been measured, except for carbazole•Ar, where it is 3.48 Å.[14] However, Neusser *et al.*[15] determined the benzene-NG distances by rotationally resolved R2PI spectroscopy. The benzene•Ar distance is slightly longer,

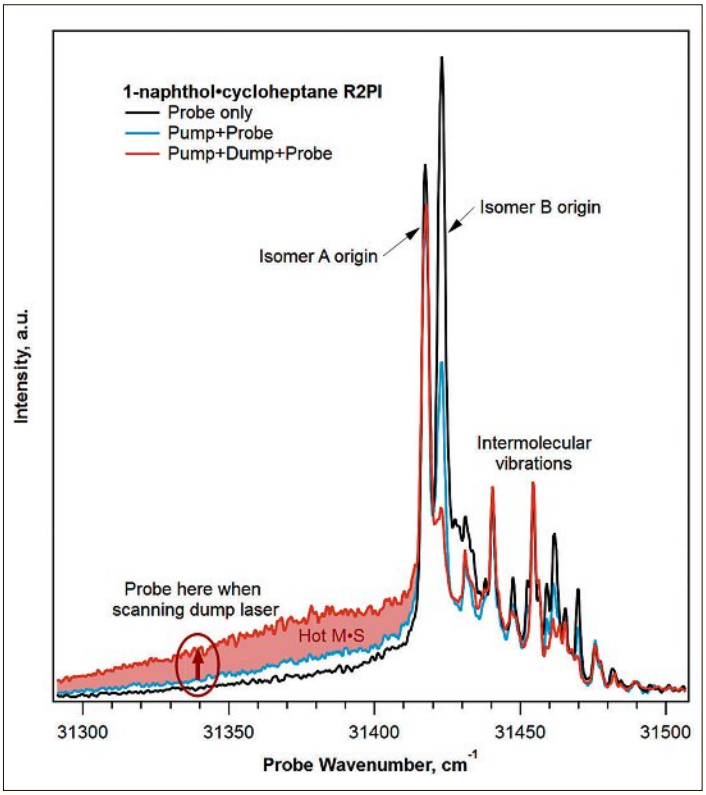

Fig. 2. Resonant two-photon ionization 'probe' spectra of the 1-naphthol•cycloheptane complex. Two isomers exist in the supersonic jet, and are denoted A and B. See the text for details.

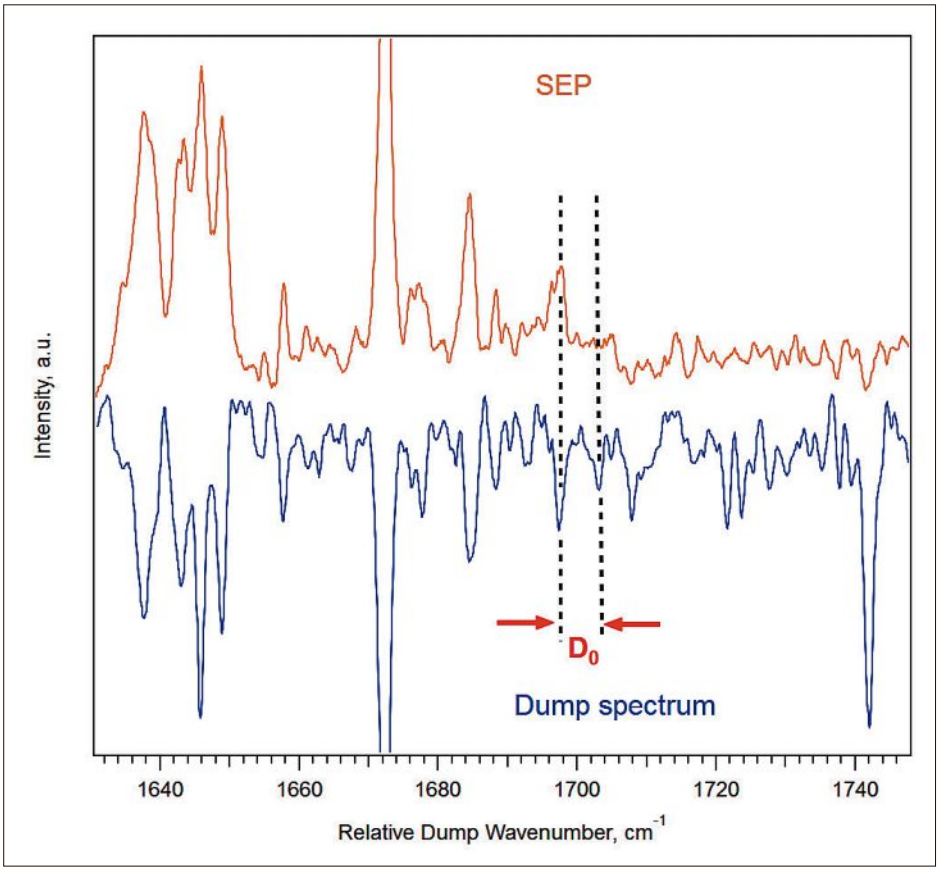

Fig. 3. Example of a SEP-R2PI dissociation energy bracketing measurement for the 1-naphthol•cyclohexane complex. The top trace shows the breakoff of the SEP spectrum of the hot complex, marked by the left dashed line. The dump spectrum of the cold complex (lower trace) continues to higher energies. The right dashed line marks the first band that appears in the bottom but not in the top spectrum. The ground state dissociation energy $D_0(S_0)$ is bracketed by the dashed lines at 1697 and 1703 cm^{-1}.

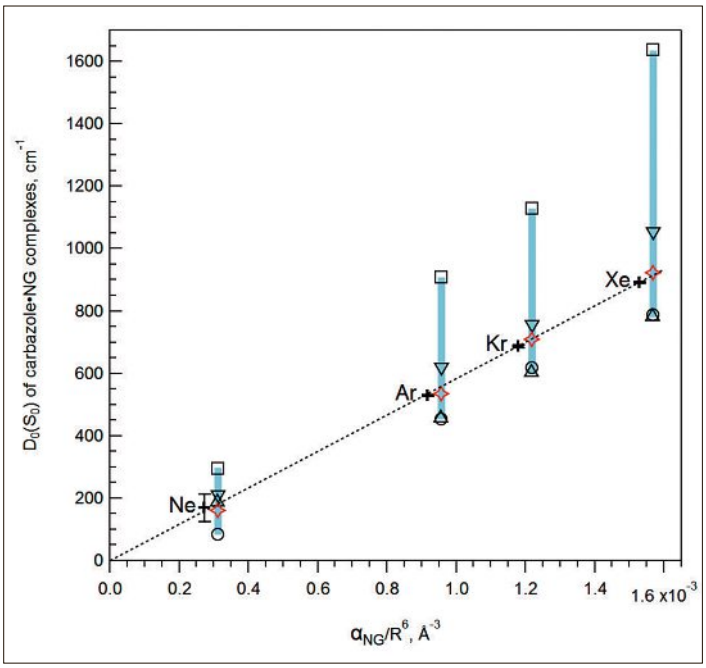

Fig. 4. SEP-R2PI dissociation energies $D_0(S_0)$ of carbazole•noble gas complexes (+ symbols with error bars) vs. the noble gas polarizability and R^{-6} distance dependence of Eisenshitz-London dispersion theory.[16] Only an upper limit was measured for carbazole•Ne, the lower limit was estimated. The D_0 values fall on a line with an x-intercept of zero, as predicted by the theory. Calculated dissociation energies (taken from Table 7 of ref. [13]) are shown in the blue bars, which are slightly offset for clarity. Δ: PBE-D3/def2-TZVP; O: SCS-CC2/aug-cc-pVTZ; □ : MP2-F12; ∇: SCS-MP2-F12; red ◊: SAPT-F12(MP2).

3.58 Å, reflecting the greater dispersion attraction of the larger carbazole. The carbazole-NG distances for the other rare gases have been correspondingly decreased by 0.1 Å from the benzene-NG values.

With these estimated carbazole-atom distances, the D_0 data in Fig. 4 closely follow a line proportional to $\alpha(NG)/R^6$. No curvature corresponding to other R^{-n} terms is visible. Carbazole has a permanent dipole moment of 1.9 D, so the dissociation energies include a dipole-induced-dipole component. However this is also proportional to R^{-6}, so it cannot be separated from the dispersion contribution in Fig. 4. Both of these interactions scale linearly with the dipole polarizability α of the NG atom. However, a symmetry-adapted perturbation-theory (SAPT) analysis[13] shows that the dispersive contribution is considerably larger than the inductive one. The ratio of (dispersion + dispersion-exchange)/(induction + induction-exchange) ranges from 71 (Ne) to 8 (Xe). Finally, it should be noted that the ionization energy correction factor of the atom-atom Eisenshitz-London dispersion equation[16] has a negligible effect on the linearity of the results in Fig. 4.

Fig. 4 also shows the D_0 values calculated using different high-level correlated *ab initio* and density functional methods, as reported in Table 7 of ref. [13]. The large scatter of the calculated values relative to experiment shows that the treatment of non-covalent interactions in intermolecular complexes of this size (15–20 second-row atoms) remains a major challenge for theory. The SAPT-F12(MP2)/aug-cc-pVTZ D_0 values in Fig. 4 (red diamonds) are the only ones within <5% of the experimental values. In this method, an MP2-F12-based correction of the inter-fragment (carbazole or NG) pair energies is added to a density-functional SAPT calculation. On the other hand, MP2-F12 itself strongly overestimates the $D_0(S_0)$ values; the SCS-CC2 and SCS-MP2-F12 methods under- and overestimate the $D_0(S_0)$ by about 15%. The dispersion-corrected density functional theory (DFT) method PBE-D3 also predicts too low values.

3. Complexes with Hydrocarbons

The $D_0(S_0)$ values of the complexes of carbazole with noble gas atoms can be understood using simple models for dispersive attraction. The picture is much less clear for M•S complexes where S is a molecule. Fig. 5 shows the experimental $D_0(S_0)$ values for 1-naphthol•cycloalkane complexes up to cycloheptane.[17] Again, the $D_0(S_0)$ values increase with the isotropic (average) polarizability $\bar{\alpha}$ of S.

However, the dissociation energies of the cyclopentane and cyclohexane complexes are identical, despite a ~20% difference in $\bar{\alpha}$ (cycloalkane).[17] In contrast to the NG complexes in Fig. 4, the $D_0(S_0)$ values fit poorly to a line that is constrained to zero intercept on the $\bar{\alpha}$ axis (dashed line). The abscissa of Fig. 5 does not include an R^{-6} factor as in Fig. 4, since there is no well-defined intermolecular distance R. This example for the 1-naphthol•cycloalkanes is not unique, the benzene•hydrocarbon series listed in Table 9 of ref. [11] also do not show a clear trend with $\bar{\alpha}$.

Clearly it is insufficient to treat molecular adsorbates as atoms by reducing their structural complexity to a single polarizability parameter. Alternative approaches should also be more efficient than the computationally expensive correlated wave function methods used above for the carbazole•NG complexes. DFT methods have been parameterized to perform very well in respect to many chemical properties and are often computationally less intensive than correlated wave function methods. However, long-range dispersion is not described by gradient-corrected (semi)local DFT methods. A number of groups have added empirical long-range dispersion corrections to DFT by generalizing the London formula to the level of atoms in the molecules, typically being an atom-pairwise sum.[18–24] While these corrections are semiclassical in character, they provide a well-defined measure of the dispersion contribution to intermolecular interactions.[18–24]

Fig. 5 includes the $D_0(S_0)$ values of the 1-naphthol•cycloalkane complexes calculated with three dispersion-corrected DFT methods. None of the complexes would be bound without the dispersion correction, and the level of agreement clearly depends on the specific functional, but overall, the dispersion corrections are quite successful. The B97-D3 method predicts D_0 values that are nearly within the experimental brackets. The atom-pairwise calculations also indicate why the $D_0(S_0)$ values of the 1-naphthol•cyclopentane and cyclohexane complexes are nearly identical.

Fig. 6 shows the B97-D3 calculated structures; the distances of the methylene groups to the naphthalene plane are seen to be different, as expected based on the different internal flexibility of cyclopentane and –hexane. In the cyclopentane complex four methylene groups are close to the naphthalene plane, while for cyclohexane only three CH_2 groups are in direct contact with the naphthalene rings; since the C-H bonds point directly down, the center of mass of cyclohexane is pushed slightly higher above the ring. Because the atom-atom dispersion energy has an

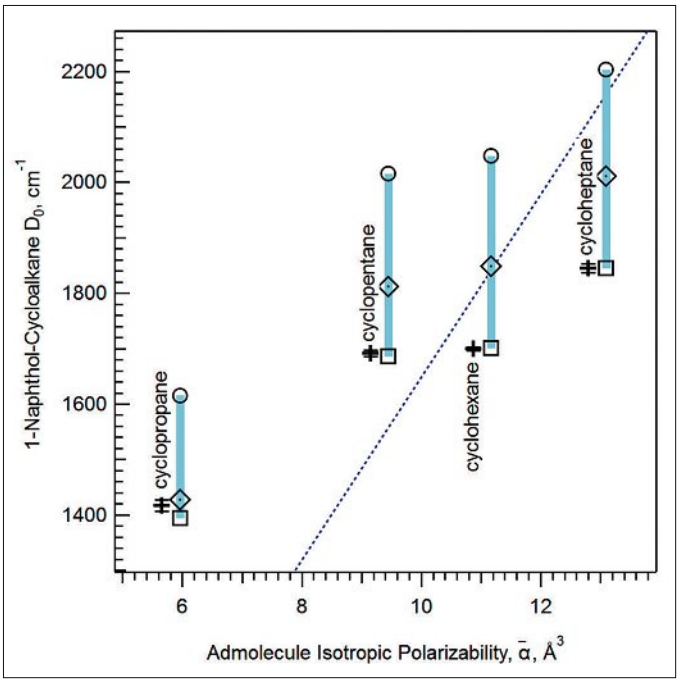

Fig. 5. SEP-R2PI dissociation energies $D_0(S_0)$ of 1-naphthol•cycloalkane complexes (+ symbols with error bars) vs. the isotropic (average) polarizability $\bar{\alpha}$ of the cycloalkanes. The dashed line is a linear fit to experiment with the x-intercept constrained to zero. The $D_0(S_0)$ values calculated with three different DFT-D methods are shown by blue bars, which are horizontally slightly offset for clarity. □: B97-D3; ◊: B3LYP-D3; O: ϖB97X-D.

R^{-6} dependence, these factors have a large effect.

Fig. 6 also shows the cumulative C and H atomic contributions to the dispersion energy, calculated with the Grimme D2 method at the geometries shown. At a given distance, the dispersive contributions of the C atoms are much larger than those of the H atoms. Due to the R^{-6} dependence, however, the H atoms that are close to the naphthalene contribute nearly as much as the C atoms to which they are bound. Up to a distance of 4.2 Å, the cyclohexane interaction is actually smaller than that of cyclopentane. The three methylene groups of cyclohexane that are farthest contribute only about 20% of the total interaction. This comparison demonstrates how the details of the intra- and intermolecular geometries combine to determine the final intermolecular energy.

4. Hydrogen-bonded Complexes of 1-Naphthol

The accurate knowledge of dissociation energies of hydrogen bonds is crucial both for the understanding of these more complex intermolecular interactions and also in order to calibrate and benchmark the (so far largely) empirical intermolecular potentials that are widely used to model and simulate the structures, folding patterns and dynamics of peptides, proteins, nucleic acids or carbohydrates in force-field-type calculations.

We have employed the SEP-R2PI method to determine ground state H-bond dissociation energies of supersonic-jet cooled H-bonded complexes.[8,11,12] As the UV chromophore we employed 1-naphthol, which is known to act as an H-donor *via* its OH group to H-acceptors such as H_2O and NH_3.[25–28] The measured $D_0(S_0)$ values for these complexes and those with methanol, ethanol, the cyclic ethers oxirane, oxetane, and the amines NH_3 and ND_3 are shown in Fig. 7 and listed in Table 1. They cover a range from 24.3 kJ/mol for H_2O up to 33.5 kJ/mol for ND_3.[8,12] While the value for oxetane is even larger, only an upper value could be experimentally determined. This reveals one of the experimental limitations of the SEP-R2PI method: Typically, the vibronic transitions exhibit decreasing Franck-Condon factors with increasing intramolecular vibrational frequency. For high enough vibrational energy, the dump transitions have such a low oscillator strength that the dump signals disappear. The point at which this happens is chromophore-dependent.

The excited-state dissociation energy, $D_0(S_1)$, can also be readily determined by adding the spectral shift of the $S_0 \rightarrow S_1$ 0_0^0 band of the M•S complex, relative to the $S_0 \rightarrow S_1$ 0_0^0 band of bare M. The $D_0(S_1)$ values are given in column 3 of Table 1 and are 5%–7% larger than the corresponding $D_0(S_0)$.

The $D_0(S_0)$ values of the H-bonded complexes are more difficult to interpret than those of the dispersively bound complexes, because there are several major contributions to the total interaction. The interactions of the permanent electrostatic moments of M and S (mainly dipole-dipole, dipole-quadrupole and quadrupole-quadrupole) typically contribute 30–50% to the binding energy; they are strongly orientation-dependent and determine the

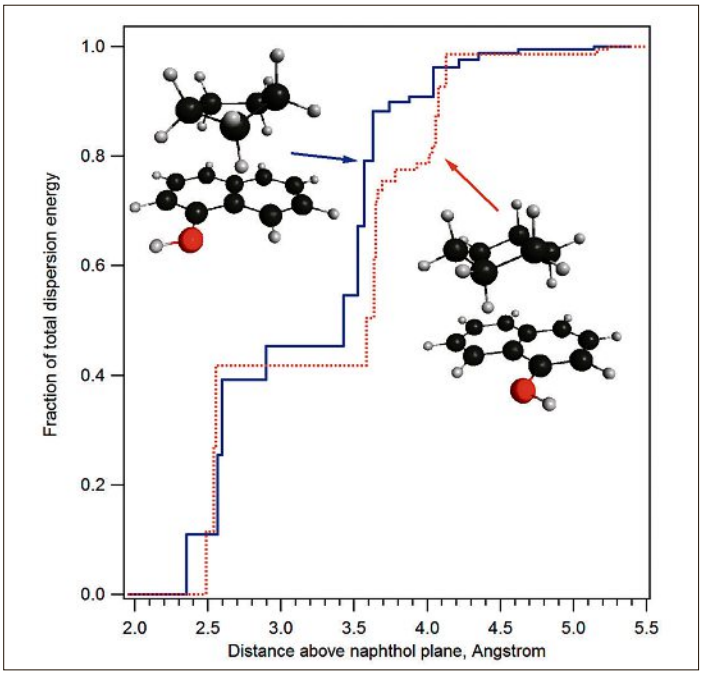

Fig. 6. Inserts: Structures of the 1-naphthol•cyclopentane and 1-naphthol•cyclohexane complexes, calculated at the B97-D3 level. The red and blue traces show the cumulative fractional contributions of the cycloalkane C and H atoms to the total D2 dispersion energy. See the text for more details.

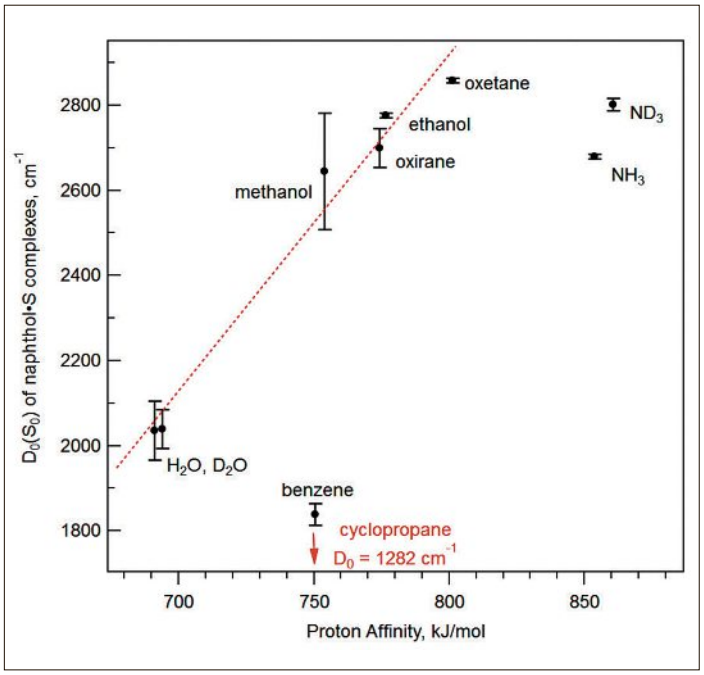

Fig. 7. SEP-R2PI dissociation energies of hydrogen-bonded M•S complexes with M = 1-naphthol, vs. the gas-phase proton affinity (PA) of the H-bond acceptor S. While the oxygen H-bond acceptors fall on a line, other classes do not. The non-classical H-bond acceptors benzene and cyclopropane have nearly identical PA values but very different dissociation energies.

relative angular orientation of the M and S moieties. Dispersive interactions contribute 40–60% of the interaction energy. Although they are often larger than the electrostatic contribution, they are weakly orientation-dependent. Finally, the inductive and charge transfer contributions are smaller, of the order of 10–20% of the interaction energy.[13]

Thus it is not surprising that no single molecular property or 'descriptor' of the H-acceptor molecules correlates well with all the dissociation energies in Table 1. Nevertheless, Fig. 7 plots $D_0(S_0)$ against the gas-phase proton affinity (PA) of the acceptors. This is often a reasonably good H-bond binding energy predictor for acceptors with large and strongly localized electron densities, such as those in the lone-pair regions of N and O. Such acceptors typically lead to 'classical' H-bonds. Indeed the correlation of $D_0(S_0)$ with PA is rather good for the series of chemically similar oxygen-containing acceptors. However, Fig. 7 shows that the amine acceptors do not follow the same correlation as the O acceptors. On the other hand, the correlation with gas-phase isotropic polarizability $\bar{\alpha}$ is rather poor for these complexes.[12] The dissociation energies of the *non-classically* H-bonded systems 1-naphthol·benzene[11] and 1-naphthol·cyclopropane[30] are also included in Fig. 7. These acceptors exhibit a smaller and less localized electron density, such as the aromatic π-electron system of benzene, or the C–C bond of cyclopropane. For these cases, the correlation with the gas-phase proton affinity breaks down completely.[12] While benzene and cyclopropane have the same proton affinity, their dissociation energies differ by about 40%.

5. Conclusions

The results discussed above demonstrate that SEP-R2PI is a flexible and accurate technique for measuring the intermolecular dissociation energies of M•S intermolecular complexes in their ground and first excited states. In many cases, the D_0 brackets are much narrower than those obtainable by alternative methods,[13,31,32] making it often the method of choice. Further advantages of the method are:

(1) It is fully spectroscopic in that the transitions utilized access well-defined vibrational levels of the chromophore. The pump transition uses the vibrationless 0-0 electronic transition, while the dump laser induces stimulated emission down

Table 1. Ground- and excited-state dissociation energies $D_0(S_0)$ and $D_0(S_1)$, for OH···O and OH···N hydrogen-bonded 1-naphthol complexes, from SEP-R2PI measurements

	$D_0(S_0)$ [kJ/mol]	$D_0(S_1)$	Ref.
1-naphthol•H_2O	24.34 ± 0.83	26.08 ± 0.83	[8]
1-naphthol-d_1•D_2O	24.39 ± 0.55	26.11 ± 0.55	[29]
1-naphthol•CH_3OH	31.6 ± 1.6	33.53 ± 1.6	[8]
1-naphthol•C_2H_5OH	33.21 ± 0.07	35.05 ± 0.07	[29]
1-naphthol•oxirane	32.30 ± 0.54	33.80 ± 0.54	[28]
1-naphthol•oxetane	>34.2	>36.4	[28]
1-naphthol•NH_3	32.06 ± 0.06	34.88 ± 0.06	[8]
1-naphthol-d_3•ND_3	33.51 ± 0.17	36.33 ± 0.17	[8]
1-naphthol•benzene	21.21 ± 0.30	22.0 ± 0.3	[11]
1-naphthol•benzene-d_6	21.27 ± 0.30	21.2 ± 0.3	[11]
1-naphthol•cyclopropane	15.35 ± 0.03	16.20 ± 0.04	[30]

to energetically narrow *intra*molecular vibrational levels of M. At the same time, it is not necessary to select specific types or symmetries of the target levels, or even to know anything about them. This is in contrast to Birge-Sponer-type methods that presuppose knowledge of the potential shape and associated vibrational assignments.

(2) From the SEP-accessed chromophore vibrational levels, energy flows into the M•S *inter*molecular motions by intracomplex M→S vibrational relaxation (IVR). Therefore, IVR is necessary and beneficial, not detrimental as in the multistep up-pumping schemes discussed in the Introduction.

(3) Apart from considerations noted below, the method does not depend on the strength of the intermolecular interaction, the structure of the M•S complex, or the spectroscopic properties of S. This allows application to a wide range of complexes and exploration of systematic series of admolecules. So far, SEP-R2PI has been used to determine the $D_0(S_0)$ of about 25 different complexes.[7–12,17,30]

(4) Thanks to mass spectrometric detection, isotopic effects on $D_0(S_0)$ can be investigated. These arise from the mass-dependent changes in the intra- and intermolecular vibrational zero-point energies. Mass-selective detection also allows the discrimination of signals from larger $M•S_n$ clusters from those of M•S. Additionally, the spectral selectivity of the narrowband pump and dump steps allows discrimination of stacked and hydrogen-bonded complex isomers, as we have shown for the 1-naphthol•cyclopropane and 1-naphthol•cycloheptane complexes.[17,30]

At the same time, the SEP-R2PI method has some limitations:

(1) Since it involves three consecutive electronic excitation/de-excitation steps, it is only practical if the chromophore transitions have large oscillator strengths, typically f_{el}>0.05.

(2) A further condition on the chromophore M is that the fluorescence quantum yield of the $S_1(v'=0)$ vibrationless level should be large, typically $\Phi_{fl} \geq 0.4$ If M undergoes rapid internal conversion or intersystem crossing from the pumped level, the overall efficiency of the SEP process becomes very low. A large fluorescence quantum yield is also useful for measuring the fluorescence spectrum of M•S when determining the upper D_0 limit.

(3) The width of the D_0 bracket depends on the density of optically accessible vibronic transitions in the dump spectrum, and on their intensities (Franck-Condon factors). These depend mainly on the chromophore M, although strongly bound M•S complexes also exhibit useful intra+intermolecular combination bands. Bracketing is often less successful if the D_0 is very low (carbazole•Ne, insufficient state density), or for very large D_0 (1-napthol•oxetane, insufficient vibronic intensity).

In an effort to obtain chemical insight, it is common to discuss intermolecular interactions in terms of molecular properties of the M and S monomers (electrostatic moments, dipole polarizability, gas-phase proton affinity, *etc.*).[3,4,13,20] In simple cases like the dispersion-dominated noble gas complexes, good correlation was observed between $D_0(S_0)$ and the dipole polarizabilities of the gas atoms $\bar{\alpha}(S)$.[7,9,10,13] In the case of larger admolecules, their proximity to and their complicated 'contact surface' with the chromophore M means that a more local description of the molecular properties becomes relevant, invalidating parametrizations in terms of a single molecular property. Particularly for the (classically and non-classically) H-bonded complexes, a good description of the interactions is only possible at the atomic scale. Also, the details of the structure of M•S become decisive, as was illustrated in section 3.

In this situation, recent developments in *ab initio* and density functional theories for the description of intermolecular interactions are very welcome.[13,20] On the other hand, the number of methods has dramatically increased, especially due to the advent of dispersion-corrected density functional schemes.[20,22] As seen in Figs 4–7, these have not yet converged to a generally reliable description of intermolecular interactions. Therefore it is necessary to benchmark the theoretical predictions against experimental results, as provided by the SEP-R2PI method.

Acknowledgements

We thank the Priority Program No. SPP1807 'Control of London dispersion interactions in molecular chemistry' of the DFG and the Swiss National Science Foundation for support (SNSF Grant No. 200021E-16040).

Received: December 29, 2016

[1] R. T. Birge, H. Sponer, *Phys. Rev.* **1926**, *28*, 259.
[2] P. M. Morse, *Phys. Rev.* **1929**, *34*, 57.
[3] G. C. Maitland, M. Rigby, E. B. Smith, W. A. Wakeham, 'Intermolecular Forces: Their Origin and Determination', Clarendon Press, Oxford, **1981**.
[4] A. J. Stone, 'The Theory of Intermolecular Forces', Clarendon Press, Oxford, **1996**.
[5] P. Maksyutenko, T. R. Rizzo, O. V. Boyarkin, *J. Chem. Phys.* **2006**, *125*, 181101.
[6] M. Grechko, O. V. Boyarkin, T. R. Rizzo, P. Maksyutenko, N. F. Zobov, S. V. Shirin, L. Lodi, J. Tennyson, A. G. Császár, O. L. Polyansky, *J. Chem. Phys.* **2009**, *131*, 221105.
[7] T. Bürgi, T. Droz, S. Leutwyler, *Chem. Phys. Lett.* **1994**, *225*, 351.
[8] T. Bürgi, T. Droz, S. Leutwyler, *Chem. Phys. Lett.* **1995**, *246*, 291.
[9] T. Bürgi, T. Droz, S. Leutwyler, *J. Chem. Phys.* **1995**, *103*, 7228.
[10] T. Droz, T. Bürgi, S. Leutwyler, *J. Chem. Phys.* **1995**, *103*, 4035.
[11] C. Wickleder, T. Droz, T. Bürgi, S. Leutwyler, *Chem. Phys. Lett.* **1997**, *264*, 257.
[12] C. Wickleder, D. Henseler, S. Leutwyler, *J. Chem. Phys.* **2002**, *116*, 1850.
[13] J. A. Frey, C. Holzer, W. Klopper, S. Leutwyler, *Chem. Rev.* **2016**, *116*, 5614.
[14] R. Sussmann, H. J. Neusser, *Chem. Phys. Lett.* **1992**, *221*, 46.
[15] H. J. Neusser, R. Sussmann, A. M. Smith, E. Riedle, T. Weber, *Ber. Bunsenges. Phys. Chem.* **1992**, *96*, 1252.
[16] R. Eisenschitz, F. London, *Eur. Phys. J. A* **1930**, *60*, 491.
[17] S. Maity, P. Ottiger, F. A. Balmer, R. Knochenmuss, S. Leutwyler, *J. Chem. Phys.* **2016**, *145*, 244314.
[18] A. Tkatchenko, M. Scheffler, *Phys. Rev. Lett.* **2009**, *102*, 73005.
[19] U. Zimmerli, M. Parrinello, P. Koumoutsakos, *J. Chem. Phys.* **2004**, *120*, 2693.
[20] S. Grimme, A. Hansen, J. G. Brandenburg, C. Bannwarth, *Chem. Rev.* **2016**, *116*, 5105.
[21] S. Grimme, *J. Comput. Chem.* **2006**, *27*, 1787.
[22] S. Grimme, *J. Comput. Chem.* **2004**, *25*, 1463.
[23] S. Grimme, J. Antony, S. Ehrlich, H. Krieg, *J. Chem. Phys.* **2010**, *132*, 154104.
[24] J.-D. Chai, M. Head-Gordon, *Phys. Chem. Chem. Phys.* **2008**, *10*, 6615.
[25] D. F. Plusquellic, X.-Q. Tan, D. W. Pratt, *J. Chem. Phys.* **1992**, *96*, 8026.
[26] L. Connell, S. Ohline, P. Joireman, T. Corcoran, P. Felker, *J. Chem. Phys.* **1991**, *94*, 4668.
[27] C. Tanner, C. Manca, S. Leutwyler, *Science* **2003**, *302*, 1736.
[28] C. Tanner, D. Henseler, S. Leutwyler, L. L. Connell, P. M. Felker, *J. Chem. Phys.* **2003**, *118*, 9157.
[29] C. Wickleder, D. Henseler, S. Leutwyler, *J. Chem. Phys.* **2002**, *116*, 1850.
[30] S. Maity, R. Knochenmuss, C. Holzer, G. Féraud, J. Frey, W. Klopper, S. Leutwyler, *J. Chem. Phys.* **2016**, *145*, 164304-1-9.
[31] H. J. Neusser, H. Krause, *Chem. Rev.* **1994**, *94*, 1829.
[32] J. E. Braun, T. Mehnert, H. J. Neusser, *Int. J. Mass Spec.* **2000**, *203*, 1.